Simultaneous Multiple Wavelength Upconversion in a Core–Shell Nanoparticle for Enhanced Near Infrared Light Harvesting in a Dye-Sensitized Solar Cell

Chunze Yuan,[†] Guanying Chen,[*,†,‡,⊥] Lin Li,[#] Jossana A. Damasco,[‡] Zhijun Ning,[†] Hui Xing,[§] Tianmu Zhang,[∥] Licheng Sun,[#] Hao Zeng,[§] Alexander N. Cartwright,[∥] Paras N. Prasad,[*,‡] and Hans Ågren[*,†]

[†]Department of Theoretical Chemistry and Biology, School of Biotechnology, Royal Institute of Technology (KTH), 10691 Stockholm, Sweden

[‡]Institute for Lasers, Photonics, and Biophotonics, [§]Department of Physics, and [∥]Department of Electrical Engineering, University of Buffalo, The State University of New York, Buffalo, New York 14260, United States

[⊥]School of Chemical Engineering and Technology, Harbin Institute of Technology, Harbin 15000, People's Republic of China

[#]Center of Molecular Devices, Department of Chemistry, School of Chemical Science and Engineering, Royal Institute of Technology (KTH), 10044 Stockholm, Sweden

S *Supporting Information*

ABSTRACT: The efficiency of most photovoltaic devices is severely limited by near-infrared (NIR) transmission losses. To alleviate this limitation, a new type of colloidal upconversion nanoparticles (UCNPs), hexagonal core–shell-structured β-NaYbF$_4$:Er^{3+}(2%)/NaYF$_4$:Nd^{3+}(30%), is developed and explored in this work as an NIR energy relay material for dye-sensitized solar cells (DSSCs). These UCNPs are able to harvest light energy in multiple NIR regions, and subsequently convert the absorbed energy into visible light where the DSSCs strongly absorb. The NIR-insensitive DSSCs show compelling photocurrent increases through binary upconversion under NIR light illumination either at 785 or 980 nm, substantiating efficient energy relay by these UCNPs. The overall conversion efficiency of the DSSCs was improved with the introduction of UCNPs under simulated AM 1.5 solar irradiation.

KEYWORDS: *upconversion, dye-sensitized solar cells, energy relay, near-infrared, nanoparticles*
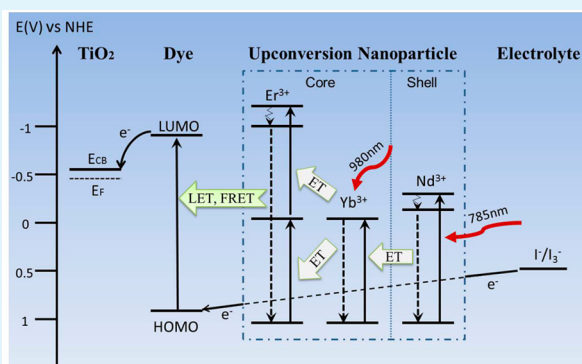
INTRODUCTION

Dye-sensitized solar cells (DSSCs) are attractive as promising solar energy harvesting devices due to many factors such as low cost, ease of fabrication, and reasonable efficiency.[1−4] The theoretical maximum efficiency of a DSSC can reach as high as around 33%.[5] However, the record efficiency of the DSSCs is still limited to ~12%, as reported by Grätzel and co-workers, despite pertinent developments during the past decade.[6] The major problem is a mismatch between the absorption spectrum of the photosensitizer and the solar irradiation spectrum.[7] In particular, the involved photosensitizer generally has an extremely limited response to near-infrared (NIR) light which constitutes almost half of the irradiated solar energy, thus severely limiting the total energy conversion efficiency of a DSSC. To date, most popular photosensitizers are designed for collection of visible light. To extend the light-collection range to the NIR region, some recent efforts have focused on the development of NIR-responsive photosensitizers for panchromatic DSSCs.[8−13] However, this type of panchromatic DSSCs

remains rather problematic, as it comes along with a low electron injection efficiency and heavily competing charge recombination leading to limited efficiency.[14] Until this point, it remains a big challenge to design a photosensitizer that can harvest both visible and NIR light.

Upconversion (UC) materials, which can convert NIR photons into visible photons[15−20] and are usually designed with core–shell structures,[35−37] have been considered as one of the promising solutions utilizing the NIR energy for DSSCs.[21−24] UC materials can absorb NIR irradiation and radiate upconverted visible emission, which can then be captured by a photosensitizer. In such a case, the photoaction spectrum will be extended to NIR light, leading to more charge carriers generated in the DSSCs.[25−27] Demopoulos and co-workers reported a Er^{3+}/Yb^{3+} codoped LaF$_3$−TiO$_2$ nano-

composite utilized as the photoanode material in DSSCs.[28] Core–double-shell-structured β-NaYbF$_4$:Er^{3+}/Yb^{3+}@SiO$_2$@ TiO$_2$ hexagonal submicroprisms have been employed in DSSCs.[29] Furthermore, a device with a heteronanostructured photoelectrochemical anode embedded in porous photonic crystals has been prepared for enhancement of NIR light-harvesting for DSSCs.[30] Recently, we reported colloidal upconversion nanoparticles (UCNPs), which could collect 980 nm NIR light as energy relay materials for DSSCs.[31] However, all of the mentioned UCNPs above only harvest a single narrow region around 980 nm, strongly limiting their NIR energy harvesting capability. It has been shown that the optimized efficiency of a solar cell combined with UC materials is proportional to the bandwidth of the employed upconverters.[32] Yet, it is nontrivial to broaden the NIR harvesting of UC materials for use in solar cells due to the f–f transition nature of lanthanide ions and some unconstructive interactions between neighboring lanthanide ions. Herein, we report the development and use of a new type of core–shell-structured β-NaYbF$_4$:Er^{3+}(2%)/NaYF$_4$:Nd^{3+}(30%) UCNPs as energy relay material for DSSCs to enhance NIR light harvesting (see Scheme 1). In addition to the NIR absorption provided by the

Scheme 1. Energy Level Illustration of the UCNPs-Doped DSSCs, Where the NIR Energy Is Converted into the Visible Spectrum Energy via the Internal Energy Transfer (ET) of UCNP, and the Upconverted Energy of UCNP is Transferred to the Photosensitizer, N719 dye, via the Processes of Fluorescence Resonance Energy Transfer (FRET) and Luminescence-Mediated Energy Transfer (LET) under Solar Illumination
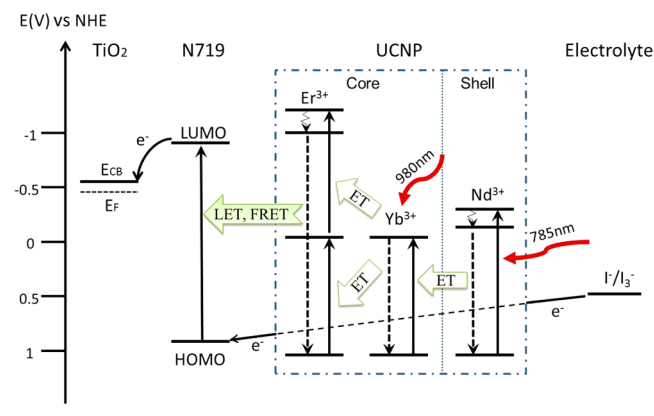
Yb^{3+} ions, this new type of UCNPs is able to harvest broader NIR light due to multiple absorption bands in the Nd^{3+} ions. The incorporation of Nd^{3+} into the shell layer spatially isolates the Nd^{3+} ions from the Er^{3+} and the Yb^{3+} ions in the core nanoparticle, avoiding cross-relaxation-induced UC quenching effects. Thus, this spatial isolation of lanthanide ions permits strong absorbing abilities of Nd^{3+} ions to be utilized, while maintaining the high upconversion efficiency of the Yb^{3+}/Er^{3+} ion pairs. Moreover, the Nd^{3+} ions in the shell are able to efficiently sensitize the Yb^{3+} ions in the core, providing a new channel to upconvert the harvested NIR light. As a consequence, this core–shell design enables efficient upconversion of NIR light excited at both Nd^{3+} ion and Yb^{3+} ion. A broad range of NIR light absorption from these core–shell UCNPs is expected to produce a pronounced effect on the efficiency of DSSCs.

■ EXPERIMENTAL SECTION

Synthesis of Upconverting Core–Shell Nanoparticles. The upconverting β-NaYbF$_4$:Er^{3+}(2%)/NaYF$_4$:Nd^{3+}(30%) core–shell nanoparticles were synthesized using a three-step procedure. The first two steps involved the synthesis of the cubic phase core (α-NaYbF$_4$:Er^{3+}) and its subsequent conversion to the hexagonal phase (β-NaYbF$_4$:Er^{3+}) based on the reported procedure.[33] The last step involved the coating of the NaYF$_4$:Nd^{3+} shell to the hexagonal core. All chemicals used in the synthesis were purchased from Sigma-Aldrich and used as received.

In a typical synthesis of the cubic core, Yb$_2$O$_3$ (0.4900 mmol) and Er$_2$O$_3$ (0.0100 mmol) were mixed with 10 mL of 50% trifluoroacetic acid in a 100 mL three-necked flask then refluxed at 95 °C until completely dissolved. The clear solution was then evaporated to dryness under Ar purge to obtain 1.0 mmol RE(CF$_3$COO)$_3$ (RE = Yb + Er) precursor. Sodium trifluoroacetate (2.0 mmol) was then added together with oleic acid (8 mL, 90% tech grade), oleylamine (8 mL, 70% tech grade), and octadecene (12 mL, 90% tech grade). The solution was then degassed at 120 °C for 30 min under Ar to remove the remaining water and oxygen. The resulting solution was then heated to 300 °C (~15 °C/min) and kept at this temperature for 30 min before naturally cooling down to room temperature. Addition of 10 mL ethanol to precipitate the nanocrystals was done followed by centrifugation at 9000 rpm for 7 min. The collected precipitate is dispersed in 10 mL hexane without further washing to avoid loss of the cubic core product.

To convert the α-NaYbF4:Er^{3+} to the hexagonal phase, 5 mL of the hexane solution containing 0.5 mmol cubic core is added to the mixture of sodium trifluoroacetate (1.0 mmol), oleic acid (10 mL), and octadecene (10 mL). Residual water and oxygen were again removed by degassing at 120 °C for 30 min under Ar. The resulting solution was then heated to 320 °C (~15 °C/min) and kept at this temperature for 30 min before naturally cooling down to room temperature. Excess amount of ethanol was then added to precipitate the nanocrystals and was centrifuged at 9000 rpm for 7 min. The collected β-NaYbF$_4$:Er^{3+}(2%) crystals were then dispersed in 5 mL of hexane.

Coating of the NaREF$_4$ shell to the hexagonal core utilized the exact steps of degassing and heating described in the synthesis of the β-NaYbF$_4$:Er^{3+}(2%) core above, except the starting solution mixture consisted of RE(CF$_3$COO)$_3$ shell precursor (0.5 mmol), β-NaYbF$_4$:Er^{3+}(2%) core (0.5 mmol), and Na(CF$_3$COO) (1.0 mmol) in 10 mL of oleic acid and 10 mL of octadecene. The RE(CF$_3$COO)$_3$ shell precursor was prepared by mixing Y$_2$O$_3$ (0.1750 mmol) and Nd$_2$O$_3$ (0.0750 mmol) with 50% concentrated trifluoroacetic acid then refluxing at 95 °C to get a clear solution. The shell precursor was obtained by evaporating the solution to dryness under Ar.

Fabrication of Solar Cells. Transparent fluorine-doped tin oxide (FTO, Solaronix TCO22-7) glass was used as substrate. FTO was sequentially cleaned in saturated sodium hydroxide isopropanol solution, absolute ethanol, and deionized (DI) water for 15 min under ultrasonic treatment. After cleaning and drying of FTO, the cleaned FTO was treated in a fresh aqueous TiCl$_4$ solution (40 mM) at 70 °C for 30 min.

Two types of TiO$_2$ films were prepared via a screen-printing method with using a commercial TiO$_2$ paste (Solaronix, Ti-Nanoxide T/SP and R/SP). One type contains only transparent layers with three times screen-printing procedure. The other type TiO$_2$ film contains transparent layers and a scattering layer. The films were sintered at 500 °C for 30 min in a muffle furnace. Then, the sintered film was post-treated in a fresh aqueous TiCl$_4$ solution (40 mM) at 70 °C for 30 min. The produced TiO$_2$ electrode provided a thickness of ~9.5 μm (~7.5 μm for transparent layer and ~2 μm for scattering layer; see Figure S2 in the Supporting Information) with a working area of 5 × 5 mm.

All TiO$_2$ films were immersed into N719 solution (3 × 10^{-4} M) in the mixture of acetonitrile and t-butyl alcohol for 24 h for the sensitization. The sensitized films were washed with ethanol solution and dried under dry air. UCNPs were deposited onto the dye-
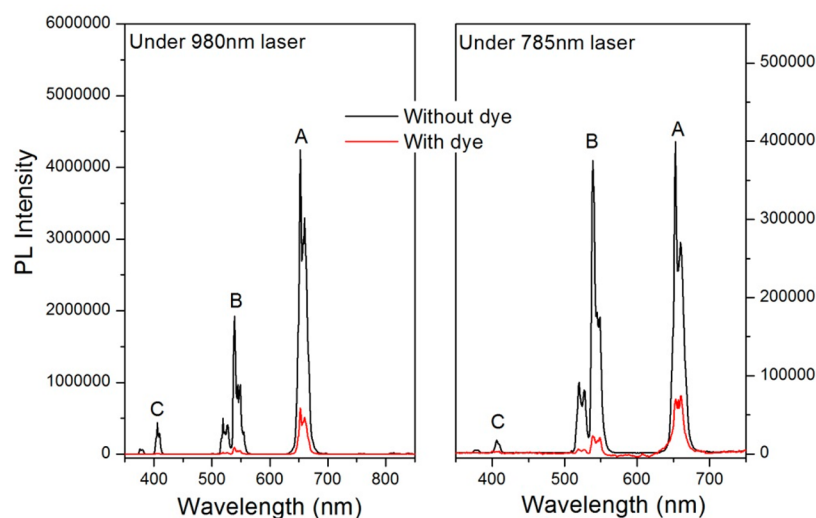
Figure 1. Photoluminescence spectra of the UCNPs (0.01 M, black line) with the addition of N719 dye (0.2 mM, red line) in the mixture solvent $CHCl_3$/acetonitrile/t-butyl alcohol = 3:1:1 (v:v:v), under the excitation at 980 nm (left) or 785 nm (right).

sensitized films simply by immersing the films into UCNPs solution (0.01 M) in hexane for 10, 30, or 60 min, following by washing with hexane solution. All the immersion and washing processes were carried out under room temperature.

A platinized FTO glass was used as counter electrode. TiO_2 films and counter electrode were sealed with a 25 μm thick Surlyn at 120 °C. There is a predrilled hole in the counter electrode, where electrolyte (0.3 M LiI, 0.03 M I_2, and 0.6 M t-butylpyridine in acetonitrile solution) was introduced into the solar cells. The hole was finally sealed with a Surlyn and a thin glass. Under each condition, at least four samples were prepared for the measurements in order to obtain a medium value as the final data.

Measurements and Equipment. The current density−voltage (I−V) characteristics were measured by using a computerized Keithley 2400 source meter. Three light sources were used: 980 nm laser (Q-photonics), 785 nm laser (Q-photonics), and sun simulator (Oriel, AM 1.5G illumination at 100 mW/cm^2). A black mask (6 × 6 mm) was used in the subsequent photovoltaic studies. The incident photon to current efficiency (IPCE) spectra were measured using a tungsten-halogen light source combined with a monochromator (Spectra Pro 2300, Acton Research), and a lock-in amplifier (SR-830, Stanford Research) by locking to the modulation frequency. UV−vis absorption spectra of UCNPs in hexane and N719 sensitized TiO_2 films were measured by using a Shimadzu UV-3600 instrument. TiO_2 films for UV−vis measurement only contain transparent layer films without the scattering layer. Photoluminescence (PL) spectra were measured by using a FluoroLog spectrofluorometer from Horiba, Jobin Yvon. Transmission electron microscopy (TEM) was performed by using a JEM-2010 instrument. The TiO_2 films were examined via field emission scanning electron microscopy (SEM) with a Hitachi SU-70 instrument at 5 kV acceleration voltage. For type 1 films, a working distance of 3 mm and 100 000 magnification was used. For type 2 films, a working distance of 3−4 mm and 50 000 magnification was used.

RESULTS AND DISCUSSION

The UV−vis absorption spectrum of the UCNPs is shown in Figure S1 in the Supporting Information. The absorption spectrum of the UCNPs exhibits six peaks consistent with the electronic transitions of the Yb^{3+} and Nd^{3+} ions. The observed peak at 980 nm corresponds to the $^2F_{7/2} \rightarrow {}^2F_{5/2}$ transition of the Yb^{3+} ion; while the remaining peaks are centered around 860, 800, 740, 580, and 520 nm, corresponding to the transitions of $^4I_{9/2} \rightarrow {}^4F_{3/2}$, $^4I_{9/2} \rightarrow {}^2H_{9/2} + {}^4F_{5/2}$, $^4I_{9/2} \rightarrow {}^4S_{3/2} + {}^4F_{7/2}$, $^4I_{9/2} \rightarrow {}^2G_{5/2, 7/2}$, and $^4I_{9/2} \rightarrow {}^4G_{7/2} + {}^2G_{9/2}$ of the

Nd^{3+}ion, respectively. The absorption bands peaked at 980, 860, 800, and 740 nm are in the NIR range. Moreover, the absorption band from the Nd^{3+} ion at 800 nm and the one from the Yb^{3+} ions at 980 nm allow the UCNPs to be excited either by a commercial 980 nm or a 795 nm laser diode source. The UC process in the Yb^{3+}/Er^{3+} ion pair is well-established, whereby the Yb^{3+} ion is first excited by ∼980 nm with subsequent transfers of photoexcited energy to the Er^{3+} ions to produce UC emissions. When the Nd^{3+} ions in the shell are excited, the absorbed energy, for example, at 785 nm, is transferred first to the Yb^{3+} ions in the core, which then sensitize the Er^{3+} ions by resonant energy transfer processes.

To investigate energy transfer between the UCNPs and the photosensitizer N719, the PL spectra of UCNPs in the absence and the presence of N719 were obtained under the excitation at 980 and 785 nm (shown in Figure 1). In the absence of N719, the UC PL spectrum of UCNPs is shown with black lines in Figure 1. As can be seen, three UC PL emissions are observed at 650 nm (peak A), 540 nm (peak B), and 406 nm (peak C). It is obvious that the PL intensity of the peak B is much lower than that of peak A under the excitation at 980 nm, while these two peaks are quite similar under the excitation at 785 nm. The discrepancy in UC PL spectra arises from the fact that the UC mechanism when exciting the Nd^{3+} ion is distinct from the one when exciting the Yb^{3+} ion. It is noted that it is not correct to compare the intensity of peak A under the excitation of 980 nm with that of 785 nm excitation, due to the different powers used for the two lasers (486 mW for 980 nm, and 300 mW for 785 nm). The high PL intensity at peak B is striking because it matches the strong absorption of the dye photosensitizer in this region (see Figure S3 in the Supporting Information, absorption spectrum of N719 on TiO_2). When the N719 dye was added to the UCNPs solution, the PL intensity decreased for all peaks (peak A−C in Figure 1, red lines. More details of this PL intensity decrease are shown in Table 1). The PL intensities for peaks B and C decreased much more than that for peak A. This is because the N719 has stronger absorption at 406 and 540 nm than at 650 nm, further leading to increased energy harvesting by the UCNPs at peaks B and C. The decreased PL intensities indicate that energy transfer between the UCNPs and the photosensitizer N719 indeed occurs.

Table 1. Extent of Decreased PL Intensity When N719 Was Added to the UCNPs Solutions

IR excitation	peak A (650 nm) decreased	peak B (540 nm) decreased	peak C (406 nm) decreased
under 980 nm	6.6 times	20 times	40 times
under 785 nm	5 times	15 times	almost all

Synthesized nanocrystals UCNPs were investigated by using TEM image shown in Figure 2. The TEM image (left, Figure 2)
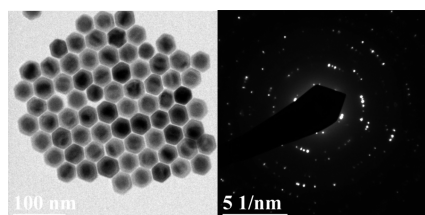
Figure 2. (Left) TEM image and (Right) selected area electron diffraction (SAED) pattern of UCNPs.

shows a clear core–shell structure of the synthesized UCNPs, with a spherelike core of 40 nm (dark contrast), and a hexagon-shape shell with thickness of ~5 nm (light contrast). This contrast between the core and the shell arises from a large difference in the atomic numbers between the Yb^{3+} ion in the core $NaYbF_4$ and the Y^{3+} ion in the shell $NaYF_4$. Moreover, these core/shell nanoparticles are highly monodisperse with an average diameter of 50 nm. The electron diffraction (SAED) pattern of the UCNPs (right, Figure 2) confirms the crystalline hexagonal structure of the resulting core/shell UCNPs. Doping of Nd^{3+} into the shell was found to be a good strategy in enhancing the UCNPs sensitization at ~800 nm by allowing the increase of Nd^{3+} concentration (~30%) without inducing significant cross-relaxations.

UCNPs were deposited on TiO_2 films and examined by a field emission scanning electron microscope (SEM). Two types of TiO_2 films were used. The first one is only a transparent TiO_2 layer with the particle size around 20 nm (TiO_2 type 1). The other film is a transparent TiO_2 layer plus a scattering layer of TiO_2. The particle size of TiO_2 in the scattering layer is around 100 nm (TiO_2 type 2). Figure 3a shows the SEM image of the surface of the N719 sensitized TiO_2 film (type 1). Mesoporous particles were uniformly and densely distributed on the surface. As can be observed in Figure 3b, spherical UCNPs (with the particles size around 50 nm) are deposited on the surface of the TiO_2 films. The particles size of UCNPs is clearly larger than the pore size of the TiO_2 film (type 1), which means that most of UCNPs are unable to infiltrate into the pores of the transparent TiO_2 layer. Therefore, most of the UCNPs were deposited on the surface of the films rather than penetrating into the internal deep layer of the films. In contrast, bigger TiO_2 particles around 100 nm were employed as a scattering layer for the TiO_2 films (Figure 3c), which appears with a big pore size and as loosely packed at the surfaces. These big pores allow UCNPs to penetrate into the scattering layer of the TiO_2 films. More UCNPs could be deposited into the films without clogging the pores (Figure 3d), which implies that the electrolyte could easily travel through this scattering layer and further react with the photosensitizer. In short, the pore size of type 1 film (transparent TiO_2) is small, limiting the infiltration
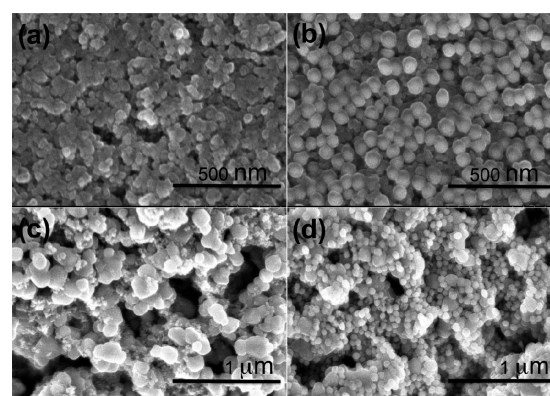
Figure 3. SEM images of the surface of the N719 sensitized TiO_2 film: (a) only transparent TiO_2 without UCNPs, (b) transparent TiO_2 with UCNPs, (c) scattering layer of TiO_2 without UCNPs, and (d) scattering layer of TiO_2 with UCNPs. The particle size of transparent TiO_2 is around 20 nm. The particle size of scattering layer of TiO_2 is around 100 nm.

of the UCNPs, while the type 2 film (scattering TiO_2) has big pore size, allowing efficient infiltration of the UCNPs.

UCNPs in the DSSCs were investigated by inspecting the current–voltage (I–V) performance of the DSSCs under illumination of a 980 nm laser (Figure 4). The I–V curve of a
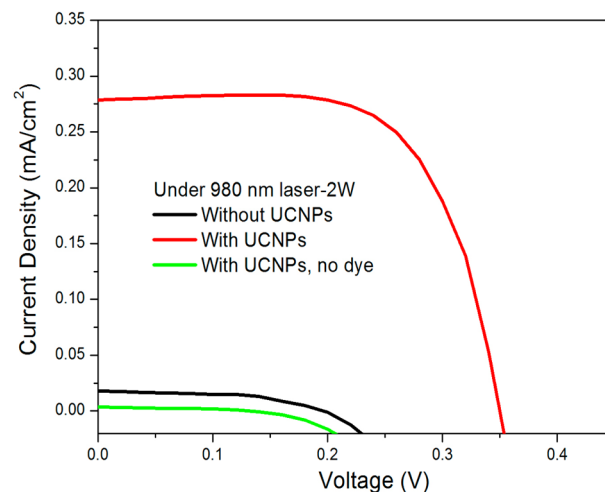
Figure 4. I–V curves of standard solar cell without UCNPs (black line), with the addition of UCNPs (red line), and control sample without photosensitizer N719 (green line) under illumination of a 980 nm laser with 2 W power.

regular DSSC without UCNPs is shown as the black line. As can be seen, the current density and the voltage are low, because the cell was measured under the illumination of a 980 nm laser, where the photosensitizer N719 could not harvest energy directly from this light source. When UCNPs was added, an enhancement in current and voltage was observed. The current density is greatly increased from 0.02 to 0.27 mA/cm². This enhancement is clearly due to the energy transfer from UCNPs to N719, after UCNPs harvest energy from the light source. But the current density is lower than that in our previous report based on NEY-1 UCNPs under the same condition.[31] This may be attributed to a relatively weak energy transfer from the UCNPs to the organic dyes. This is because larger size UCNPs is used in this work, which is mostly

positioned in the scattering layer of the TiO_2 film (consult Figure 3). This results in a longer distance between the UCNPs and the dyes, thus producing a lower energy transfer rate between them. Meanwhile, a control experiment was carried out, which is a solar cell lacking photosensitizer N719 (green line). It can be seen that this control sample without N719 shows almost no photocurrent, indicating that UCNPs alone cannot (or barely) generate photocurrent. In other words, the high photocurrent of the cell with UCNPs and N719 predominately derives from the energy relay from the UCNPs to photosensitizer N719, rather than by a direct electron transfer from the UCNPs to TiO_2.[34] Moreover, the photocurrent was enhanced with the increase of power density of light (Figure S4, Supporting Information). The heating is generated simultaneously under light illumination, especially using a high-power laser. It should be noted that N719 would be desorbed at high working temperature, which leads to the descent of photovoltaic performance of N719-based DSSCs.[38] Since the photocurrent in this work was mostly dependent on the illumination density, the heating effect was reflected on the photovoltage (Figure S4, Supporting Information). The photovoltage of the cells without UCNPs was decreased with the increase of power density of the light. However, the photovoltage of the UCNP-based cells was just decreased when laser power is up to 2 W, which indicates that the UCNPs can protect N719 from heating desorption to some extent.

The $I-V$ curves of solar cells were also studied under illumination of a 785 nm laser, shown in Figure 5. The $I-V$
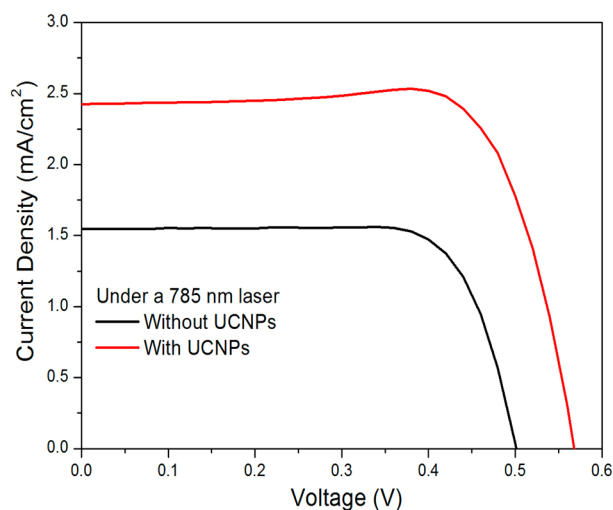

Figure 5. $I-V$ curves of standard solar cell (black line) and with the addition of UCNPs (red line) under illumination of a 785 nm laser with 25 mW power.

curve of a regular DSSC without UCNPs is shown as the black line, while the one for a DSSC with UCNPs is shown as a red line. As one can see, when UCNPs were introduced, an enhancement in both the current and the voltage was clearly observed. The current density is increased from 1.55 to 2.43 mA/cm^2. Compared to the cell without UCNPs, the overall conversion efficiency is improved by 80% under a low laser power of merely 25 mW. This efficiency increase is clearly a direct result of energy transfer from UCNPs to N719, after the UCNPs harvested energy from the light source. It is noted that the photosensitizer N719 has an edge response at 785 nm (consult the absorption spectrum of N719 on TiO_2 in Figure

S3 in the Supporting Information), thus producing a higher background current density (1.55 mA) and voltage than the values of the DSSC without UCNPs under the illumination of a 980 nm laser (consult Figure 4). In addition, other factors, such as that UCNPs could act as light scattering particles, might also contribute to the enhancement of performance of the solar cell.

As noted above, we have successfully demonstrated enhanced NIR light harvesting using upconversion at 980 nm due to the absorption of Yb^{3+} ion, and at 785 nm due to the absorption of Nd^{3+} ion. However, it is inappropriate to directly compare the improved performance of solar cells under the excitation of 980 nm with that under the excitation of 785 nm, as different powers of the two lasers are employed (2 W for 980 nm, and 25 mW for 785 nm). If considering the improved efficiency per megawatt of laser irradiation using UCNPs, a higher improvement number of 35 $\mu A/cm^2$/mw is observed in the DSSC for light illumination at 785 nm than 0.125 $\mu A/cm^2$/mw for light illumination at 980 nm. This is because UCNPs give more PL intensity at the 540 nm (peak B) under the excitation of 785 nm than that under the excitation of 980 nm (consult discussion in the previous section, Figure 1), and because the N719 dye has a maximal absorption at around 540 nm (Figure 3S, Supporting Information).

It is important to maintain the overall performance of the solar cells under the standard condition referring to the simulated solar irradiation of AM 1.5. Therefore, the effect of UCNPs on the overall performance of the solar cells was investigated under this standard condition, as shown in Figure 6
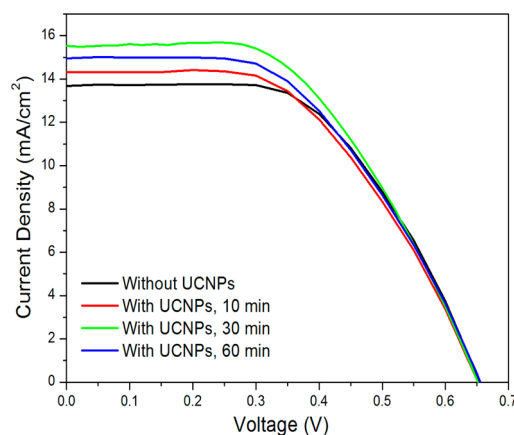

Figure 6. $I-V$-curves of solar cells without (black line) and with the use of UCNPs for the preparation of 10 (red line), 30 (green line), and 60 min (blue line) under simulated AM 1.5 irradiation.

and Table 2. The preparation of the UCNPs deposited onto dye-sensitized TiO_2 films at different times was also included in this study. Although the voltage largely seems to remain the same for the different cells, there are observable differences in the current density between the cells. When the deposition

Table 2. Performance of Solar Cells without and with the Use of UCNPs for the Preparation of 10, 30, and 60 min

device	J_{sc} [mA/cm^2]	V_{oc} [V]	FF	η [%]
without UCNPs	13.7	0.66	0.55	4.95
with UCNPs, 10 min	14.3	0.66	0.51	4.85
with UCNPs, 30 min	15.5	0.65	0.52	5.24
with UCNPs, 60 min	15.0	0.66	0.51	5.01

process of UCNPs ran for 10 min, a higher photocurrent, 14.3 mA/cm^2, was observed than when the device was without UCNPs (13.7 mA/cm^2). This enhancement might be partly due to increased absorption in the NIR region when UCNPs was introduced. Moreover, other reasons such as light scattering by UCNPs might also be responsible for the enhancement of photocurrent.[31] When the deposition time was prolonged to 30 min, a further increase in the photocurrent (15.5 mA/cm^2) was observed compared to the device with UCNPs deposited for 10 min. This enhancement could be simply because more UCNPs were deposited on the TiO$_2$ film when longer-time processing was carried out. However, the photocurrent decreased to 15.0 mA/cm^2, when the deposition time was further prolonged to 60 min. As discussed in the previous section concerning Figure 3, it is known that N719 dyes and UCNPs are mainly localized in the transparent layer and the scattering layer, respectively. Therefore, this decrease might be caused by the UCNPs blocking the pores at the interface between the transparent layer and the scattering layer of the TiO$_2$ film, when an increased number of UCNPs were introduced into the TiO$_2$ film. As a result, the UCNPs blocking effect limits the movement of the electrolyte to transparent layer, and thus lowers the efficiency of the solar cells. The fill factor (FF) also decreases when UCNPs are introduced. The incident photon to current efficiency (IPCE) spectra of the DSSCs without and with the use of the UCNPs for 30 min deposition are shown in Figure 7. The IPCE obviously
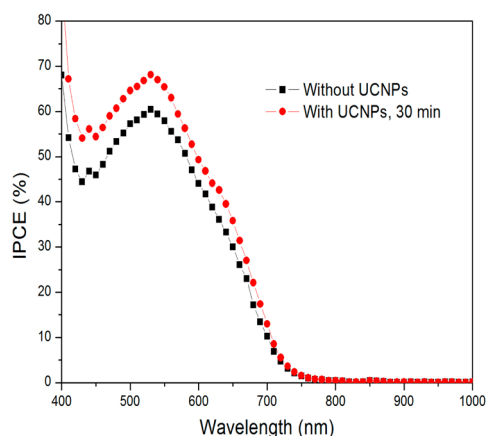

Figure 7. IPCE of solar cells without (black line) and with the use of UCNPs for the preparation of 30 min (red line).

increases in the visible region with a limited increase in the NIR region. This indicates that the enhancement of photocurrent under AM 1.5 sun irradiation might be due to other reasons such as scattering of the UCNPs as described in our previous publication.[31] Here we also present the reproducibility of the $I-V$ result based on ~30 samples for each device for comparison under AM 1.5 sun. As shown in Figure S8 in the Supporting Information, the average photocurrent was increased from 13 to 15.2 mA/cm^2 by depositing UCNPs for 30 min, which resulted in the improvement of the average efficiency from 4.5 to 5.2%.

CONCLUSIONS

In conclusion, we have investigated binary upconversion of a new type of core−shell UCNPs in DSSCs for enhanced NIR light harvesting. These UCNPs consist of a hexagonal NaYbF$_4$:Er^{3+}(2%)/NaYF$_4$:Nd^{3+}(30%) core−shell structure, which is able to harvest NIR light through single band absorption from Yb^{3+} ions as well as from multiple band absorptions from Nd^{3+} ions, providing broad NIR harvesting. The spatial isolation of lanthanide ions in the core−shell design enables the new absorbing abilities of the Nd ions, while maintaining the high upconversion efficiency of the Er^{3+} ions. The photocurrent of the solar cells employing UCNPs was found to be improved as compared to that of the solar cells without UCNPs under the illumination at 785 nm (for excitation of Nd^{3+}), the illumination at 980 nm (for excitation of Yb^{3+}), as well as under simulated solar irradiation AM 1.5. It is clear that the NIR response of the DSSCs has been enhanced and broadened by this new type of UCNPs. However, the results for the solar cell under simulated solar irradiation AM 1.5 indicate that the scattering introduced by UCNPs also contributes to the enhancement of photocurrent under this specific condition. This work provides a paradigm for broadening the NIR absorption of UCNPs toward improving the efficiency of DSSCs. The further improvement of performance of UCNP-assistant DSSCs can be expected to occur on the basis of improvements of the upconversion efficiency of the UCNPs, which, for example, can be achieved through coupling to localized surface plasmons from surrounding metallic structures.[39,40]

ASSOCIATED CONTENT

Supporting Information

(1) UV−vis absorption spectrum of UCNPs dispersed in hexane; (2) SEM image of cross section of UCNPs nanoparticles deposited on dye (N719) sensitized TiO$_2$ film; (3) UV−vis absorption spectra of N719 on transparent TiO$_2$ film with and without UCNPs; (4) $I-V$ curves of standard solar cell and with the addition of UCNPs under the illumination of a 980 nm laser with different power; (5) fluorescence spectra of the UCNPs under 800 nm laser; (6) dependence of the intensity of UC PL peaks at 520, 540, and 650 nm on the power density of excitation at 980 and 798 nm for UCNPs; (7) mechanisms of upconversion emissions in the UCNPs. This material is available free of charge via the Internet at http://pubs.acs.org.

AUTHOR INFORMATION

Corresponding Authors

*(G.C.) E-mail: guanying@buffalo.edu.
*(P.N.P.) E-mail: pnprasad@buffalo.edu.
*(H.A.) E-mail: agren@theochem.kth.se. Fax: +46 8 55378416. Tel: +46 8 55378590.

Notes

The authors declare no competing financial interest.

■ REFERENCES

(1) O'Regan, B.; Grätzel, M. A Low-Cost, High-Efficiency Solar Cell Based on Dye-Sensitized Colloidal Titanium Dioxide Films. *Nature* **1991**, *353*, 737−740.

(2) Hagberg, D. P.; Yum, J. H.; Lee, H.; De Angelis, F.; Marinado, T.; Karlsson, K. M.; Humphry-Baker, R.; Sun, L.; Hagfeldt, A.; Gratzel, M.; Nazeeruddin, M. K. Molecular Engineering of Organic Sensitizers for Dye-Sensitized Solar Cell Applications. *J. Am. Chem. Soc.* **2008**, *130*, 6259−6266.

(3) Grätzel, M. Recent Advances in Sensitized Mesoscopic Solar Cells. *Acc. Chem. Res.* **2009**, *42*, 1788−1798.

(4) Hagfeldt, A.; Boschloo, G.; Sun, L.; Kloo, L.; Pettersson, H. Dye-Sensitized Solar Cells. *Chem. Rev.* **2010**, *110*, 6595−6663.

(5) Shockley, W.; Queisser, H. J. Detailed Balance Limit of Efficiency of p-n Junction Solar Cells. *J. Appl. Phys.* **1961**, *32*, 510−519.

(6) Yella, A.; Lee, H.-W.; Tsao, H. N.; Yi, C.; Chandiran, A. K.; Nazeeruddin, M. K.; Diau, E. W.-G.; Yeh, C.-Y.; Zakeeruddin, S. M.; Grätzel, M. Porphyrin-Sensitized Solar Cells with Cobalt (II/III)-Based Redox Electrolyte Exceed 12% Efficiency. *Science* **2011**, *334*, 629−634.

(7) Hardin, B. E.; Hoke, E. T.; Armstrong, P. B.; Yum, J.-H.; Comte, P.; Torres, T.; Fréchet, J. M. J.; Nazeeruddin, M. K.; Grätzel, M.; McGehee, M. D. Increased Light Harvesting in Dye-Sensitized Solar Cells with Energy Relay Dyes. *Nat. Photonics* **2009**, *3*, 406−411.

(8) Nazeeruddin, M. K.; Pechy, P.; Renouard, T.; Zakeeruddin, S. M.; Humphry-Baker, R.; Comte, P.; Liska, P.; Cevey, L.; Costa, E.; Shklover, V.; Spiccia, L.; Deacon, G. B.; Bignozzi, C. A.; Graetzel, M. Engineering of Efficient Panchromatic Sensitizers for Nanocrystalline TiO$_2$-Based Solar Cells. *J. Am. Chem. Soc.* **2001**, *123*, 1613−1624.

(9) Chiba, Y.; Islam, A.; Watanabe, Y.; Komiya, R.; Koide, N.; Han, L. Dye-Sensitized Solar Cells with Conversion Efficiency of 11.1%. *Jpn. J. Appl. Phys., Part 2* **2006**, *45*, L638−L640.

(10) Reddy, P. Y.; Giribabu, L.; Lyness, C.; Snaith, H. J.; Vijaykumar, C.; Chandrasekharam, M.; Lakshmikantam, M.; Yum, J.-H.; Kalyanasundaram, K.; Graetzel, M.; Nazeeruddin, M. K. Efficient Sensitization of Nanocrystalline TiO$_2$ Films by a Near-IR-Absorbing Unsymmetrical Zinc Phthalocyanine. *Angew. Chem., Int. Ed.* **2007**, *46*, 373−376.

(11) Hao, Y.; Yang, X.; Cong, J.; Tian, H.; Hagfeldt, A.; Sun, L. Efficient Near Infrared D-π-A Sensitizers with Lateral Anchoring Group for Dye-Sensitized Solar Cells. *Chem. Commun.* **2009**, 4031−4033.

(12) Tian, H.; Yang, X.; Chen, R.; Hagfeldt, A.; Sun, L. A Metal-Free "Black Dye" for Panchromatic Dye-Sensitized Solar Cells. *Energy Environ. Sci.* **2009**, *2*, 674−677.

(13) Kinoshita, T.; Dy, J. T.; Uchida, S.; Kubo, T.; Segawa, H. Wideband Dye-Sensitized Solar Cells Employing a Phosphine-Coordinated Ruthenium Sensitizer. *Nat. Photonics* **2013**, *7*, 535−539.

(14) Ning, Z.; Fu, Y.; Tian, H. Improvement of Dye-Sensitized Solar Cells: What We Know and What We Need to Know. *Energy Environ. Sci.* **2010**, *3*, 1170−1181.

(15) Chen, G.; Qiu, H.; Prasad, P. N.; Chen, X. Upconversion Nanoparticles: Design, Nanochemistry, and Applications in Theranostics. *Chem. Rev.* **2014**, *114*, 5161−5214.

(16) Chen, G.; Ohulchanskyy, T. Y.; Kumar, R.; Agren, H.; Prasad, P. N. Ultrasmall Monodisperse NaYF$_4$:Yb^{3+}/Tm^{3+} Nanocrystals with Enhanced Near-Infrared to Near-Infrared Upconversion Photoluminescence. *ACS Nano* **2010**, *4*, 3163−3168.

(17) Xie, X.; Gao, N.; Deng, R.; Sun, Q.; Xu, Q. H.; Liu, X. Mechanistic Investigation of Photon Upconversion in Nd^{3+}-Sensitized Core-Shell Nanoparticles. *J. Am. Chem. Soc.* **2013**, *135*, 12608−12611.

(18) Wen, H.; Zhu, H.; Chen, X.; Hung, T. F.; Wang, B.; Zhu, G.; Yu, S. F.; Wang, F. Upconverting Near-Infrared Light Through Energy Management in Core-Shell-Shell Nanoparticles. *Angew. Chem., Int. Ed.* **2013**, *52*, 13419−13423.

(19) Zhong, Y.; Tian, G.; Gu, Z.; Yang, Y.; Gu, L.; Zhao, Y.; Ma, Y.; Yao, J. Elimination of Photon Quenching by a Transition Layer to Fabricate a Quenching-Shield Sandwich Structure for 800 nm Excited Upconversion Luminescence of Nd^{3+}-Sensitized Nanoparticles. *Adv. Mater.* **2014**, *26*, 2831−2837.

(20) Wang, Y. F.; Liu, G. Y.; Sun, L. D.; Xiao, J. W.; Zhou, J. C.; Yan, C. H. Nd^{3+}-Sensitized Upconversion Nanophosphors: Efficient in vivo Bioimaging Probes with Minimized Heating Effect. *ACS Nano* **2013**, *7*, 7200−7206.

(21) Chen, G.; Seo, J.; Yang, C.; Prasad, P. N. Nanochemistry and Nanomaterials for Photovoltaics. *Chem. Soc. Rev.* **2013**, *42*, 8304−8338.

(22) Chen, G.; Yang, C.; Prasad, P. N. Nanophotonics and Nanochemistry: Controlling the Excitation Dynamics for Frequency Up- and Down-Conversion in Lanthanide-Doped Nanoparticles. *Acc. Chem. Res.* **2013**, *46*, 1474−1486.

(23) de Wild, J.; Meijerink, A.; Rath, J. K.; van Sark, W. G. J. H. M.; Schropp, R. E. I. Upconverter Solar Cells: Materials and Applications. *Energy Environ. Sci.* **2011**, *4*, 4835−4848.

(24) Zhang, J.; Shen, H.; Guo, W.; Wang, S.; Zhu, C.; Xue, F.; Hou, J.; Su, H.; Yuan, Z. An Upconversion NaYF4:Yb^{3+},Er^{3+}/TiO$_2$ Core−Shell Nanoparticle Photoelectrode for Improved Efficiencies of Dye-Sensitized Solar Cells. *J. Power Sources* **2013**, *226*, 47−53.

(25) Wang, J.; Wu, J.; Lin, J.; Huang, M.; Huang, Y.; Lan, Z.; Xiao, Y.; Yue, G.; Yin, S.; Sato, T. Application of Y$_2$O$_3$:Er^{3+} Nanorods in Dye-Sensitized Solar Cells. *ChemSusChem* **2012**, *5*, 1307−1312.

(26) Liu, M.; Lu, Y.; Xie, Z. B.; Chow, G. M. Enhancing Near-Infrared Solar Cell Response Using Upconverting Transparentceramics. *Sol. Energy Mater. Sol. Cells* **2011**, *95*, 800−803.

(27) van der Ende, B. M.; Aarts, L.; Meijerink, A. Lanthanide Ions as Spectral Converters for Solar Cells. *Phys. Chem. Chem. Phys.* **2009**, *11*, 11081−11095.

(28) Shan, G. B.; Demopoulos, G. P. Near-Infrared Sunlight Harvesting in Dye-Sensitized Solar Cells via the Insertion of an Upconverter-TiO$_2$ Nanocomposite Layer. *Adv. Mater.* **2010**, *22*, 4373−4377.

(29) Liang, L.; Liu, Y.; Bu, C.; Guo, K.; Sun, W.; Huang, N.; Peng, T.; Sebo, B.; Pan, M.; Liu, W.; Guo, S.; Zhao, X. Z. Highly Uniform, Bifunctional Core/Double-Shell-Structured Beta-NaYF4:Er^{3+}, Yb^{3+} @ SiO$_2$@TiO$_2$ Hexagonal sub-Microprisms for High-Performance Dye Sensitized Solar Cells. *Adv. Mater.* **2013**, *25*, 2174−2180.

(30) Su, L. T.; Karuturi, S. K.; Luo, J.; Liu, L.; Liu, X.; Guo, J.; Sum, T. C.; Deng, R.; Fan, H. J.; Tok, A. I. Photon Upconversion in Hetero-Nanostructured Photoanodes for Enhanced Near-Infrared Light Harvesting. *Adv. Mater.* **2013**, *25*, 1603−1607.

(31) Yuan, C. Z.; Chen, G. Y.; Prasad, P. N.; Ohulchanskyy, T. Y.; Ning, Z. J.; Tian, H. N.; Sun, L. C.; Agren, H. Use of Colloidal Upconversion Nanocrystals for Energy Relay Solar Cell Light Harvesting in the Near-Infrared Region. *J. Mater. Chem.* **2012**, *22*, 16709−16713.

(32) Briggs, J. A.; Atre, A. C.; Dionne, J. A. Narrow-Bandwidth Solar Upconversion: Case Studies of Existing Systems and Generalized Fundamental Limits. *J. Appl. Phys.* **2013**, *113*, 124509.

(33) Mai, H. X.; Zhang, Y. W.; Si, R.; Yan, Z. G.; Sun, L. D.; You, L. P.; Yan, C. H. High-Quality Sodium Rare-Earth Fluoride Nanocrystals: Controlled Synthesis and Optical Properties. *J. Am. Chem. Soc.* **2006**, *128*, 6426−6436.

(34) Chang, J.; Ning, Y.; Wu, S.; Niu, W.; Zhang, S. Effectively Utilizing NIR Light Using Direct Electron Injection from Up-Conversion Nanoparticles to the TiO$_2$ Photoanode in Dye-Sensitized Solar Cells. *Adv. Funct. Mater.* **2013**, *23*, 5910−5915.

(35) Chen, F.; Bu, W.; Zhang, S.; Liu, X.; Liu, J.; Xing, H.; Xiao, Q.; Zhou, L.; Peng, W.; Wang, L.; Shi, J. Positive and Negative Lattice Shielding Effects Co-existing in Gd(III) Ion Doped Bifunctional Upconversion Nanoprobes. *Adv. Funct. Mater.* **2011**, *21*, 4285−4294.

(36) Wang, F.; Liu, X. Recent Advances in the Chemistry of Lanthanide-Doped Upconversion Nanocrystals. *Chem. Soc. Rev.* **2009**, *38*, 976−989.

(37) Li, Z.; Zhang, Y.; Jiang, S. Multicolor Core/Shell-Structured Upconversion Fluorescent Nanoparticles. *Adv. Mater.* **2008**, *20*, 4765−4769.

18024

dx.doi.org/10.1021/am504866g | *ACS Appl. Mater. Interfaces* 2014, 6, 18018−18025

(38) Wang, P.; Zakeeruddin, S. M.; Moser, J. E.; Nazeeruddin, M. K.; Sekiguchi, T.; Grätzel, M. A Stable Quasi-Solid-State Dye-Sensitized Solar Cell with an Amphiphilic Ruthenium Sensitizer and Polymer Gel Electrolyte. *Nat. Mater.* **2003**, *2*, 402−407.

(39) Sun, Q. C.; Mundoor, H.; Ribot, J. C.; Singh, V.; Smalyukh, I. I.; Nagpal, P. Plasmon-Enhanced Energy Transfer for Improved Upconversion of Infrared Radiation in Doped-Lanthanide Nanocrystals. *Nano Lett.* **2014**, *14*, 101−106.

(40) Lu, D.; Cho, S. K.; Ahn, S.; Brun, L.; Summers, C. J.; Park, W. Plasmon Enhancement Mechanism for the Upconversion Processes in NaYF$_4$:Yb^{3+},Er^{3+} Nanoparticles: Maxwell versus Forster. *ACS Nano* **2014**, *8*, 7780−7792.

18025

dx.doi.org/10.1021/am504866g | *ACS Appl. Mater. Interfaces* 2014, 6, 18018−18025